Published in final edited form as:
Immunity. 2013 March 21; 38(3): 555–569. doi:10.1016/j.immuni.2013.02.012.

Recruitment of Beneficial M2 Macrophages to Injured Spinal Cord Is Orchestrated by Remote Brain Choroid Plexus

Ravid Shechter[1,7,*], **Omer Miller**[1,7], **Gili Yovel**[1,7], **Neta Rosenzweig**[1], **Anat London**[1], **Julia Ruckh**[1], **Ki-Wook Kim**[2], **Eugenia Klein**[3], **Vyacheslav Kalchenko**[4], **Peter Bendel**[5], **Sergio A. Lira**[6], **Steffen Jung**[2], and **Michal Schwartz**[1,*]

[1]Department of Neurobiology, The Weizmann Institute of Science, Rehovot 76100, Israel

[2]Department of Immunology, The Weizmann Institute of Science, Rehovot 76100, Israel

[3]The Irving and Cherna Moskowitz Center for Nano and Bio Nano Imaging, The Weizmann Institute of Science, Rehovot 76100, Israel

[4]Department of Veterinary Resources, The Weizmann Institute of Science, Rehovot 76100, Israel

[5]Department of Chemical Research Support, The Weizmann Institute of Science, Rehovot 76100, Israel

[6]Immunology Institute, Mount Sinai School of Medicine, New York, NY 10029-6574, USA

SUMMARY

Monocyte-derived macrophages are essential for recovery after spinal cord injury, but their homing mechanism is poorly understood. Here, we show that although of common origin, the homing of proinflammatory (M1) and the “alternatively activated” anti-inflammatory (M2) macrophages to traumatized spinal cord (SC) was distinctly regulated, neither being through breached blood-brain barrier. The M1 macrophages ($Ly6c^{hi}CX3CR1^{lo}$) derived from monocytes homed in a CCL2 chemokine-dependent manner through the adjacent SC leptomeninges. The resolving M2 macrophages ($Ly6c^{lo}CX3CR1^{hi}$) derived from monocytes trafficked through a remote blood-cerebrospinal-fluid (CSF) barrier, the brain-ventricular choroid plexus (CP), via VCAM-1-VLA-4 adhesion molecules and epithelial CD73 enzyme for extravasation and epithelial transmigration. Blockage of these determinants, or mechanical CSF flow obstruction, inhibited M2 macrophage recruitment and impaired motor-function recovery. The CP, along with the CSF and the central canal, provided an anti-inflammatory supporting milieu, potentially priming the trafficking monocytes. Overall, our finding demonstrates that the route of monocyte entry to central nervous system provides an instructional environment to shape their function.

[*]Correspondence: ravid.shechter@weizmann.ac.il (R.S.), michal.schwartz@weizmann.ac.il (M.S.).
[7]These authors contributed equally to this work

SUPPLEMENTAL INFORMATION

Supplemental Information includes Supplemental Experimental Procedures and four figures and can be found with this article online at http://dx.doi.org/10.1016/j.immuni.2013.02.012.

INTRODUCTION

Infiltration of circulating monocytes after mechanical injury to the central nervous system (CNS) has been generally assumed to reflect mechanical damage to the parenchymal blood-brain barrier (BBB). Nevertheless, at early stages after mechanical injury, there is no direct evidence for escape of cellular elements across the breached BBB, whose disruption is assessed by dye or protein leakage; rather, several studies have shown parenchymal infiltration of monocytes at the subacute phase when the BBB is resealed. In addition, blood-derived macrophages contribute to CNS repair, in part by displaying resolving M2 phenotype (Kigerl et al., 2009; Rapalino et al., 1998; Shechter et al., 2009; Yin et al., 2006). Thus, the posttraumatic CNS entry, of at least some macrophages, seems to represent controlled recruitment needed for repair.

Outside the CNS, the phenotype of macrophages, derived from circulating monocytes homing to injured tissues (hereafter abbreviated as monocyte-macrophages), reflects two phases. The initial phase is characterized by Ly6c^{hi}CX3CR1^{lo} monocyte-macrophages, corresponding to the “classically activated” (M1) cells, which have been shown to possess proinflammatory, phagocytic, and proteolytic functions, essential for damaged tissue digestion and debris removal. The second phase is associated with Ly6c^{lo}CX3CR1^{hi} monocyte-macrophages, “alternatively activated” (M2) macrophages, which are anti-inflammatory in nature and are involved in tissue regeneration, growth, angiogenesis, and matrix deposition, thereby supporting tissue remodeling (Arnold et al., 2007; Nahrendorf et al., 2007). It is still unclear whether the distinct macrophage populations are an outcome of monocyte recruitment in two waves (Nahrendorf et al., 2007) or in situ phenotypic conversion of the already recruited cells (Arnold et al., 2007).

In the context of the CNS, which is separated from the circulation by a system of barriers, a fundamental question is how such cells gain access to the injured CNS parenchyma. Here, we studied the recruitment of monocyte-macrophages to spinal cord (SC) parenchyma after mechanical injury. Two monocyte-macrophage populations were found in the traumatized SC, corresponding to the M1 and M2 classes. The M1 monocyte-macrophages were found to derive from monocytes that entered the traumatized SC via CCL2 through the adjacent SC leptomeninges, whereas the M2 cells came from monocytes that trafficked through the brain-ventricular choroid plexus (CP), via VCAM-1-VLA4 and CD73. We further demonstrate that the CP-entry route is an M2-supporting milieu.

RESULTS

Two Distinct Populations of Monocyte-Macrophages Are Actively Recruited to the Injured SC Parenchyma

To follow the route of monocyte entry into the SC after trauma, we employed the contusive model of spinal cord injury (SCI), of moderate severity, which resulted in an average motor recovery of 4.4 ± 0.3 (n = 38) according to Basso Motor Score (BMS) (Basso et al., 2006). To specifically follow the infiltrating monocyte-derived cells, distinct from CNS-resident microglia, we used bone marrow (BM) chimeric mice, in which head-protected irradiated C57BL/6J recipients were reconstituted with labeled *Cx3cr1*$^{GFP/+}$ BM cells (henceforth

termed *Cx3cr1*$^{GFP/+}$ chimeras). Head-shielded chimeras, in the absence of SCI, exhibit no noticeable monocyte entry to the brain or SC (Shechter et al., 2009). Moreover, irradiation of SC does not affect monocyte recruitment (Ajami et al., 2007). Nevertheless, because it has been argued that the BM chimeric model (though without shielding) is confounded by some unavoidable artifacts (Ajami et al., 2007; Mildner et al., 2007), we confirmed our findings by experimental models that involved neither irradiation nor hematopoietic stem cell transplantation.

Cx3cr1$^{GFP/+}$ chimeras were subjected to SCI, and the excised SCs were analyzed by flow cytometry. Monocyte-macrophages could barely be detected in the lesion site at the first day postinjury (day 0), a time when the BBB is most severely breached (demonstrated by dye extravasation) (Noble and Wrathall, 1989), though hemorrhage occurred (measured by erythrocyte presence) (Figure 1A). The monocyte-macrophages expressed the macrophage and microglial differentiation marker Iba-1 (Figure 1B) and were previously found by us to express other macrophage markers, including Mac-3 and F4/80 (Shechter et al., 2009). Quantitative analysis revealed accumulation of two distinct subsets with different kinetics, first Ly6c^{hi}*Cx3cr1*-GFP^{lo} monocyte-macrophages, and subsequently Ly6c^{lo}*Cx3cr1*-GFP^{hi} monocyte-macrophages (Figure 1B). At day 7, the Ly6c^{lo}*Cx3cr1*-GFP^{hi} monocyte-macrophages expressed characteristic M2 surface markers (Dectin1, interleukin-4 receptor α chain [IL-4Rα], CD206-Mannose receptor) and anti-inflammatory cytokines (IL-10 and TGF-β), whereas the Ly6c^{hi}*Cx3cr1*-GFP^{lo} monocyte-macrophages expressed the proinflammatory cytokines IL-1β and tumor necrosis factor-α (TNF-α) (Figure 1C). Quantitative real-time PCR (qRT-PCR) of the two populations separately sorted from injured (day 5) parenchyma confirmed that the Ly6c^{lo}*Cx3cr1*-GFP^{hi} and the Ly6c^{hi}*Cx3cr1*-GFP^{lo} subsets displayed M2 and M1 characteristics, respectively (Figure 1D).

Next, we tested the effect of pertussis toxin (Ptx), an inhibitor of $G_{\alpha i}$-mediated chemokine-receptor signaling, on monocyte-macrophages homing to the injured SC. Injured CD45.1^{+} mice were intravenously injected 1 day after injury with CD115^{+} monocytes (isolated from *Cx3cr1*$^{GFP/+}$CD45.2 animals) either Ptx treated or untreated (3×10^6 cells per recipient) (Shechter et al., 2009). Flow cytometric analysis of recipient mouse tissues 2 days after transfer showed that whereas untreated monocytes homed to the injured SC, the Ptx pretreatment almost completely prevented monocyte accumulation in the injured SC, without diminishing their numbers in the blood (Figure 1E). Thus monocyte entry into the injured SC parenchyma relies on an active mechanism.

Considering the parenchymal blood-spinal cord barrier vasculature (the spinal analogy to the BBB vasculature) as a possible site for active monocyte entry, SCs of injured *Cx3cr1*$^{GFP/+}$ chimeras were excised after transcardial perfusion and were analyzed by immunohistochemistry. Monocytes were barely detected in association with parenchymal blood vessels within the lesion site or its surroundings (Figure 1F). We also did not observe during the first 14 days “perivascular cuffs,” a microscopically identifiable structure in which leukocytes accumulate between the basement membranes of the parenchymal vasculature, a typical feature of BBB transmigration (Takigawa et al., 2010). Though we cannot exclude infrequent events of BBB crossing, the above led us to search for alternative site(s) and pathway(s) for monocyte entry. The leptomeninges and the CP, recently

identified as CNS entry sites for leukocytes (Bartholomäus et al., 2009; Reboldi et al., 2009), were therefore examined.

The SC Leptomeninges Facilitate Homing to the Lesion Site of M1 Monocyte-Macrophages

Considering its anatomical proximity to the lesion site, we tested the SC leptomeninges. A reduced immunostaining for the tight junction molecule occludin expressed by endothelial cells was seen in whole-mount SC leptomeninges, isolated at day 1 post-injury, thus revealing fenestration in endothelial sealing (Figure 2A). Immunohistochemical analyses as well as quantitative flow cytometry of SC leptomeninges dissected from injured *Cx3cr1*$^{GFP/+}$ chimeras revealed the postinjury homing of GFP^{+} monocytes to the leptomeninges adjacent to the injury site (Figures 2B–2D). This was verified in nonchimeric models by intravenously injecting injured mice with either GFP^{+}CD115^{+} monocytes (the day of injury) or PE-conjugated CD11b antibodies (1 day before injury) (Figure S1 available online). The meningeal homing monocytes were primarily of the Ly6c^{hi}*Cx3cr1*-GFP^{lo} phenotype (Figure S1). No significant post-trauma recruitment was observed in SC leptomeninges distal to the site, cerebral meninges, or parenchyma of the distal SC or the brain (Figure S1).

The chemokine CCL2 (MCP-1) is known to facilitate recruitment of Ly6c^{hi} monocytes, which are CCR2^{+}, to lesion sites outside and within the CNS (Mildner et al., 2007), so we tested whether CCL2 blocking affected monocyte homing through the leptomeninges. *Cx3cr1*$^{GFP/+}$ chimeras were intraperitoneally injected with CCL2 blocking antibodies (2H5) or with IgG isotype controls on the day of SC contusion. The SC leptomeninges were analyzed by flow cytometry 1 day later (peak monocyte homing; Figure 2D). CCL2 antibody treatment significantly reduced monocyte homing of Ly6c^{hi}*Cx3cr1*-GFP^{lo} type to the leptomeninges with no effect on blood populations (Figure 2E). We repeated the experiment by administering the antibodies on the day of injury and 48 hr later and analyzed the injured SC on day 5, when the two monocyte-macrophage subtypes were detectable. CCL2 antibodies caused a significant reduction, specifically in the M1 (Ly6c^{hi}*Cx3cr1*-GFP^{lo}) monocyte-macrophages, with no effect on the appearance of M2 (Ly6c^{lo}*Cx3cr1*-GFP^{hi}) monocyte-macrophages at the lesion site (Figure 2F). To strengthen the relationship between the monocyte-macrophages found in the injured parenchyma and their entry gate, in an independent experiment we concurrently tested the lesion site along with the two potential gates at day 5; whereas the injured parenchyma and the covering leptomeninges showed reduced monocytic infiltration, specifically of the Ly6c^{hi}*Cx3cr1*-GFP^{lo} subset, the choroid plexus showed no change (Figure S1).

Healing M2 Monocyte-Macrophages in the Injured Spinal Cord Are Recruited through the Choroid Plexus

The above results led us to consider a distinct route for M2 monocyte-macrophage recruitment; we focused on the brain ventricular CP, despite its anatomical distance. Examination of brain sections stained with cresyl violet revealed irregular CP morphology at day 1 after injury (Figure 3A), a sign for blood-cerebrospinal fluid barrier (BCSFB) breaching. Immunostaining for tight junction molecules (Zo-1 and occludin) of the CP dissected several hours or 1 day after SCI revealed patches of disrupted epithelial tight

junction organization (Figures 3B and 3C), which was not seen in CP dissected from uninjured mice. Intact vessels were seen in such patches (Figure 3B), ruling out mechanical perturbation during tissue isolation. qRT-PCR of dissected CP confirmed reduced expression after injury of *Ocln*, encoding Occludin (Figure 3C).

Evaluating the CP of SC-injured *Cx3cr1*$^{GFP/+}$ chimeras revealed injury-induced homing of GFP^{+} monocytes (Figures 3D–3G). Although basal amount of monocytes were found in the CP of uninjured animals, a burst of freshly recruited GFP^{+} monocytes to the CP was seen within the first hours posttrauma (Figure 3G). Thereafter, the amount returned close to the basal surveillance quantities. However, some degree of subsequent influx through the CP probably continued. Circulating myeloid homing to the CP after SCI was verified in nonchimeric models by intravenous injection either of CD115^{+} monocytes (GFP^{+} or DIR labeled; 4 hr after contusion) or of PE-conjugated CD11b antibody (1 day before injury) to spinally injured mice (Figure S2).

The monocytes seen at the CP of *Cx3cr1*$^{GFP/+}$ chimeras were mainly of the Ly6c^{lo}*Cx3cr1*-GFP^{hi} type (Figure S2). These cells included both CP-surveying monocytes and the M2-commited or precursor cells en route to the site, which were indistinguishable based on these markers. CP-Ly6c^{lo}*Cx3cr1*-GFP^{hi} cells expressed the M2 markers Dectin-1, IL-4Rα, and CD206 (Figure S2). Importantly, these CP GFP^{+} cells, unlike the resident CP myeloid population or their progenitors (Anandasabapathy et al., 2011), expressed the monocytic marker CD115 and lacked the macrophage differentiation marker Mac-3 and the microglial and macrophage (including resident CP macrophage [Chinnery et al., 2010]) marker Iba-1 (Figures 3H and 3I).

qRT-PCR of excised CP for measurement of expression of adhesion molecules and chemokine genes revealed dynamic and selective changes in response to SCI (Figure 3J). *Cx3cl1* (Fractalkine), *Vcam1*, and *Nt5e* (encoding CD73) showed a transient elevation during the first day after injury. Notably, the CP of uninjured *Cx3cr1*$^{GFP/+}$ chimeras and wild-type mice showed no differences in the expression of these key immune-guiding molecules (Figure S2). Simultaneous multiplex analysis for various myeloid-specific chemoattractants revealed that macrophage colony-stimulating factor (M-CSF), the ligand of CD115, was the predominant factor expressed in the CP and the one that showed the highest elevation after injury (Figures 3K and S2). These changes were specific to the CP; the excised SC exhibited its own distinct pattern of chemokine changes (Figure S2).

We focused on the enzyme CD73 and the integrin ligand VCAM-1 as potential homing determinants for monocytes crossing through the CP. Immunohistochemical analysis confirmed the selective expression of these two molecules in the CP after SCI during the first few days after the injury (Figure S3). High and uniform expression of CD73 was noted in choroidal epithelium (Figure 4A), but not in the CP vasculature and not in parenchymal or leptomeningeal vessels of either the brain or the SC at all tested time points (Figure S3). Increased reactivity of CD73 in the CP epithelium was noted in the first few days (d0–d2) after the injury, in line with gene expression data (*Nt5e*) (Figure 3J). CD73 was previously shown to be exclusively expressed within the mouse CNS in the cuboidal epithelial lining of the CP (and not in CNS endothelium), facilitating epithelial transmigration during

experimental autoimmune encephalomyelitis (EAE) (Mills et al., 2008). CD73 is also expressed by leukocytes (Mills et al., 2008) but not monocytes (Thomson et al., 1990). We verified that circulating monocytes were devoid of CD73 after SCI (Figure 4B), in line with reported results after ischemic injury (Bönner et al., 2012).

To block CD73-dependent trafficking, we systemically injected (for 14 days) α,β methylene-ADP (APCP), a pharmacological CD73 inhibitor (Synnestvedt et al., 2002). A significant reduction in monocyte-macrophages at the lesion site of CD45.1→CD45.2 BM chimeric mice was observed (Figure 4C). This effect was reproduced in *Cd73*$^{-/-}$ mice; cell recruitment was traced either by in situ labeling of the cells with CFSE 24 hr before the injury (Figure 4D) or by monitoring CD45^{hi}CD11b^{hi} populations at the lesion site (Figure S3; Sedgwick et al., 1991). No reduction of blood-circulating monocytes was detected in APCP-treated mice or in *Cd73*$^{-/-}$ mice (Figures 4C and 4D).

We next examined VCAM-1 involvement in trafficking. VCAM-1 was induced in CP capillaries during the first few days after the insult (Figures 4E and S3) but not on parenchymal vessels at the lesion site nor on the leptomeninges vessels of the SC (at the lesion site or distally) or the brain (Figure S3), as previously reported (Kalderon, 2005; Schnell et al., 1999). From day 7 onward, some scattered VCAM-1 immunoreactivity was noted at the site of injury. Intravenous administration of blocking antibodies directed to VCAM-1 (MK2.7 clone) or its counterreceptor, Very Late Antigen-4 (VLA-4; α4β1) (PS2 clone), to *Cx3cr1*$^{GFP/+}$ chimeric mice immediately and 48 hr after SC insult resulted in a reduction to 50% of monocyte-macrophages at the lesion site (day 5 after injury) (Figure 4F). IgG isotype-matched antibodies were used as controls. Reduction was verified in a nonchimeric system by monitoring CD45^{hi}CD11b^{hi} expression (Figure S3). A reduction in GFP^{+} cells was also found in the CP and CSF after VLA-4 antibody treatment (Figure S3) but not in the leptomeninges adjacent to the lesion (Figure S3). Notably, the significant reduction at the lesion site by the blocking of the VCAM-1-VLA-4 interaction was restricted to the Ly6c^{lo}*Cx3cr1*-GFP^{hi} and not the Ly6c^{hi}*Cx3cr1*-GFP^{lo} monocyte-macrophage population (Figure 4G). Blocking antibodies (clone M1/70) directed to CD11b, an integrin that is expressed by monocytes and can potentially interact with ICAM-1 in the CP, had no effect on either overall homing or that of a specific monocyte-macrophage subset to the injured SC (Figure 4H).

Because monocyte-macrophages promote recovery via IL-10 production (Shechter et al., 2009), we tested whether blockage of CP-homing determinants would skew the cytokine milieu within the lesion site. Injured mice received, as above, neutralizing antibodies to VCAM-1-VLA-4 interaction or APCP. Spinally injured *Cd73*$^{-/-}$ mice were also analyzed. Multiplex protein analysis of the excised SC (day 7) revealed a selective reduction of IL-10 and IL-13 in the treated groups, relative to the relevant controls (Figure 5A). Under these experimental conditions, the overall cytokine milieu was shifted toward a proinflammatory one, as determined by qRT-PCR for several cytokines (Figure 5B).

Motor function recovery after SCI is tightly dependent on the numbers of monocyte-macrophages (Shechter et al., 2009). We therefore tested whether blocking these CP-homing determinants would impair recovery. Mice were subjected to SCI, randomly divided into

groups, and treated as above. Motor function analyses of the hind limbs starting from day 1 postinjury, a time point at which the average score of all groups was similar, revealed from day 3 onward impairment of recovery by specific VCAM-1-VLA-4 blocking antibodies relative to the controls (Figure 5C). In another set of experiments, which included injured mice receiving APCP or PBS and a group of age-matched *Cd73*$^{-/-}$ mice (with similar group average scores at the starting point [d1]), reduced recovery was similarly observed from day 4 onward in the *Cd73*$^{-/-}$ mice and in the APCP-treated mice, relative to PBS-treated wild-type mice (Figure 5C). The timing of motor score impairment correlated with the kinetics of M2 monocyte-macrophage accumulation at the lesion site (Figure 1B). On day 21 after the injury, the SCs were analyzed for lesion size by Luxol fast blue and Nissl staining; treatments interrupting CD73 activity or the VCAM-1-VLA-4 interaction resulted in extended lesion size, suggesting increased spread of damage (Figure 5D). Thus, blocking the CP-guiding determinants VCAM-1-VLA-4 and CD73 resulted in reduced M2 recruitment, proinflammatory milieu, and impaired functional recovery.

The CSF Provides an M2-Supportive Pathway for Infiltrating Monocytes

Homing through the CP to the injured SC parenchyma requires, beyond the migration across the CP, anterograde trafficking through the CSF and/or the central canal, a CSF-filled space that runs longitudinally through the SC and is continuous with the ventricular spaces. Immunohistochemical analysis of injured *Cx3cr1*$^{GFP/+}$ chimeras revealed the presence of GFP^{+} monocytes in the meninges connecting the CPs and upstream the three apertures in the fourth ventricle, through which the ventricular system communicates with the subarachnoid space (foramen of Magendie and Luschka) (Figure 6A). Such cells could not be detected in uninjured mice. Flow cytometric analysis of CSF samples aspirated from nonchimeric *Cx3cr1*$^{GFP/+}$ mice through the cisterna magna revealed the appearance of numerous GFP^{+} cells (monocyte characteristics are shown in Figure S4) 24 hr after injury (Figure 6B), reaching 50% of the leukocytes in the CSF on day 3 (Figure 6C); GFP^{+} monocytes were barely detectable in the CSF a few hours after trauma or in uninjured mice. Analysis of spinal cord sections of *Cx3cr1*$^{GFP/+}$ chimeras revealed the presence of GFP^{+} cells also throughout the central canal (Figure 6A). Such cells could not be detected in uninjured mice. In injured *Cx3cr1*$^{GFP/+}$ chimeras, multiprocess and ameboid GFP^{+} cells were associated with the apical and luminal ependyma, respectively, of the central canal (marked with Hoechst dye or the ependymal marker Vimentin) (Figures 6D and 6E), possibly reflecting active migration. Scanning electron microscopy of the opened central canal, clearly identified by its cuboidal ependymal lining, revealed cells with typical leukocyte morphology (Figure S4) that were not seen in uninjured controls.

The injury-induced trafficking of leukocytes along the central canal correlated with its morphological changes and activation. The central canal was dilated by approximately 45% in close proximity to the lesion site relative to uninjured (1,766 ± 118) on days 1, 3, and 7 postinjury (2,562 ± 171; 2,294 ± 103; and 2,547 ± 141 μm^2, respectively; n = 4 mice each; ANOVA, F = 9.3, p = 0.0018), possibly reflecting CSF flow disturbance within the central canal (Radojicic et al., 2007). Adjacent to the lesion site, the central canal exhibited increased vimentin (Figures 6F and 6D) and GFAP immunoreactivity (not shown) and contained in its lumen a vimentin-immunoreactive fiber structure (Figure 6D). Numerous

GFP$^+$ cells were colocalized with these fibers (Figure 6D), possibly facilitating their migration. Moreover, elevated expression of the integrin ligand ICAM-1 and the chemokine Cxcl12 (SDF-1), in the first few days postinjury (day 0, 2, 3), was noted at the luminal surface of the central canal in close proximity to the lesion site but not rostally (Figure 6F).

To establish that the monocytes that trafficked through the CSF and central canal corresponded to the M2 monocyte-macrophages found in the injured SC parenchyma, we injected into the cisterna magna (the site of CSF flow after circulating in the brain ventricles) a nontoxic polymerizing agent (Matrigel) to mechanically block CSF flow (Slobodian et al., 2007). The Matrigel deposit was restricted to the cisterna magna and the fourth ventricle and did not spread to the lower compartments (Figure S4). Such a treatment did not evoke signs of inflammation at the site of needle insertion, adjacent to the ventricles, or at the SC and the leptomeninges (Figure S4). Matrigel injection caused brain ventricular enlargement, with no detectable anatomical changes in the SC parenchyma or meninges, below the Matrigel injection site (Figure S4). Flow cytometric analysis assessed 1 week after the SCI and Matrigel injection revealed a significant reduction in GFP$^+$ monocyte-macrophages (in *Cx3cr1*$^{GFP/+}$ chimeras) (Figure 6G) or in CD11b^{hi}CD45^{hi}-expressing cells (in nonchimeric mice) at the lesion site (Figure S4). Subpopulation analysis revealed that the reduction was selective for only Ly6c^{lo}*Cx3cr1*-GFP^{hi} monocyte-macrophages at the lesion site (Figure 6H), suggesting that the CP-CSF pathway orchestrates the specific recruitment of M2 monocyte-macrophages to the lesion.

We next tested whether such an extended “detour” to the lesion site through the CP and the CSF could potentially provide an environment supportive of M2 commitment. Simultaneous Multiplex analysis (by Luminex) revealed that whereas the lesion site was predominated by proinflammatory cytokines, the CP and the CSF continuously exhibited an anti-inflammatory bias (Figure 7A). IL-13, an M2 inducer (Gordon and Taylor, 2005), was the dominant cytokine in both the CP and the CSF. TGF-β and IL-10 were abundant in the CSF and CP, respectively (Figure 7A). The CP maintained its anti-inflammatory profile after SCI, unlike the lesion site, which displayed an elevation of proinflammatory cytokines (Figure 7B) and transient reduction in TGF-β expression (Figure 7C). Of the TGF-β family, the CSF expressed only the TGF-β2 isoform, shown to mediate immune deviation in immune-privileged organs (Streilein, 2003). Immunolabeling for TGF-β revealed its high expression in the CP vasculature, but not in any other brain area (Figure 7D), and along the central canal of the injured SC (Figure 7E). The CP also expressed *Vip* and *Thbs1*, previously shown to promote immune deviation in immune-privileged sites (Figure 7F; Streilein, 2003).

Finally, based on the unique environment of the CSF, we tested whether direct intracerebroventricular (ICV) injection of naive CD115$^+$ monocytes isolated from the BM (>80% Ly6c^{hi}) would be sufficient to support functional recovery. Monocyte administration (day 3) to the CSF of SC-injured mice resulted in improved hind limb motor function recovery (Figure 7G) and decreased lesion size (Figure 7H), thereby demonstrating that the CSF compartment supports the differentiation of beneficial monocyte-derived cells.

DISCUSSION

In this study we have shown that monocyte recruitment to injured SC parenchyma is coordinated through two sites. The brain ventricular CP orchestrates trafficking of monocytes that locally mature to healing anti-inflammatory (M2) monocyte-macrophages, and the adjacent SC leptomeninges support trafficking of monocytes that mature to proinflammatory M1 monocyte-macrophages.

Outside the CNS, monocytes homed to injured tissue by direct extravasation from parenchymal-embedded vasculature. In the CNS, such entry would necessitate breaching the BBB. Although we cannot exclude escape of some cells, the present study suggests that in the acute phase of the response after SCI, the critical time for recovery, monocytes rarely home via parenchymal vessels. It seems that the mechanical insult itself does not trigger BBB activation. Yet, in the chronic phase, the prolonged parenchymal inflammation eventually “inflames” the BBB, leading to immune invasion; integrins are induced (Kalderon, 2005) and perivascular cuffing is observed (Takigawa et al., 2010) at 2–4 weeks posttrauma.

The CP, a ventricular BCSFB compartment with a villous structure, facilitates CNS immunosurveillance (Ransohoff et al., 2003). Along this pathway, leukocytes extravasate across the endothelium, interact with the tightly connected epithelial cells, and enter the CSF. Though investigated primary in the context of T lymphocytes (Mills et al., 2008; Reboldi et al., 2009), recent studies demonstrate that CP myeloid cells exchange with blood precursors (which are not monocytes) (Anandasabapathy et al., 2011; Chinnery et al., 2010) and that monocyte invasion to the CP occurs after head trauma (Szmydynger-Chodobska et al., 2012). Here, we suggest that the CP supports trafficking of “healing” cells to remote traumatized CNS site by serving as a selective and “phenotype-shaping gate” for monocytes en route to the lesioned parenchyma. Such M2 monocyte-macrophages secreted anti-inflammatory cytokines needed for microglial arrest, thereby limiting spread of damage as is essential for recovery (Shechter et al., 2009). Tissue remodeling (Shechter et al., 2011), axonal regeneration (Yin et al., 2006), and cell renewal were also supported by monocyte-macrophages but occurred at a later stage.

Similarly to wound healing outside the CNS (Arnold et al., 2007; Nahrendorf et al., 2007), two waves of monocyte-macrophages, corresponding to M1 and M2, were identified here to operate in the injured SC, but via distinct routes. The two gates were activated on the same timescale, so the sequential waves seen at the lesion sites could reflect the distinct pathway lengths and migration rates.

It seems that the microenvironment within CNS lesion does not allow local conversion to an M2 phenotype, in line with the inability of activated resident microglia to attain a resolving phenotype at this critical stage (Shechter et al., 2009). Similarly, myelin debris at the SC lesion site, which can potentially trigger M2 commitment (Boven et al., 2006), promotes an inflammatory response by phagocytic macrophages (Sun et al., 2010). Our results, however, do not argue against potential conversion (Arnold et al., 2007) at the injured CNS site

beyond this critical reparative time window. This explains why recruitment through the CP-CSF, which primes M2 commitment, is supportive for repair.

Integrating our previous findings that CCR2-depleting antibodies impair healing and amplify microglial inflammation (Shechter et al., 2009) with the current observations suggests that both M1 and M2 originate from a common circulating $CCR2^{+}Ly6c^{hi}$ monocytic precursor, though only M1 is recruited via its ligand CCL2. In EAE, interference with CCR2 guidance also selectively impairs the recruitment of the $Ly6c^{hi}CX3CR1^{lo}$ subset, leaving the reciprocal subpopulation unchanged (Saederup et al., 2010). Because it was mainly studied in EAE, in which M1 outnumber M2, CCL2 has been viewed as the sole "ticket" to the CNS for monocytes (Mildner et al., 2009).

CP trafficking was found here to require a unique set of homing determinants including the integrin VLA-4-VCAM-1 interaction and the adenosine catalyzing enzyme CD73. Unlike CD73's role in preventing endothelial crossing, CD73-dependent CP transmigration involves adenosine-mediated induction of the chemokine fractalkine (Mills et al., 2012). Fractalkine is a known chemoattractant of monocytes, specifically of the $CX3CR1^{hi}$ subset (Nahrendorf et al., 2007), found here in the CP; both fractalkine and $CX3CR1^{hi}$ cells were elevated in the CP of SC-injured mice.

The CP was found here to be predominated by the $CX3CR1^{hi}$ monocytic subset and was found to support M2 differentiation. In addition, the entire CP-CSF pathway was found as an M2 milieu, possibly priming trafficking monocytes to their M2 commitment prior to their arrival at the lesion site. Such a process might involve a selection or priming of monocytes at the CP gate and further education thereafter. Because bypassing the CP by injection of the primary $CCR2^{+}Ly6c^{hi}$ cells to the CSF still benefited repair, our results argue in favor of an M2-educative mechanism along the entire CP pathway. Additional studies in mice reveal that intracerebroventricular (ICV)-injected $CCR2^{+}$ human monocytes home to lesion sites and locally express IL-10 (E. Yoles, S. Snider, M. Tolmasove, A. Ruben, O. Gore, S. Har-Nof, O.M., M. Hadani, and M.S., unpublished data). Human CSF has been shown in vitro to suppress effector T cell function and to promote a "deviated" macrophage phenotype (Wilbanks and Streilein, 1992). Importantly, although we suggest that the CP route biases the commitment of the trafficking monocytes, final M2 maturation occurs at the lesion site via interaction with the local extracellular matrix (Shechter et al., 2011).

The M2-educative property of the CP route seems to contradict the suggested role of CP entry in EAE induction (Reboldi et al., 2009). It is possible that in inflammation-induced pathologies such as EAE, unlike in "sterile injurious" ones, either pathogenic cells take advantage of CNS surveillance process or the educative nature of this CP-CSF pathway is malfunctioning. In support of the former conjecture, CCL20, which has been found to facilitate CP entry of pathogenic Th17 cells (Reboldi et al., 2009), is constitutively expressed, even in the absence of disease, possibly reflecting its role in CNS immunosurveillance. One possibility is surveillance by T regulatory (Treg) cells, known to express CCR6, the chemokine receptor to CCL20 (Kleinewietfeld et al., 2005). Moreover, CCR6-CCL20 interactions guide monocyte recruitment into other epithelial tissues such as

the mucosa or skin (Le Borgne et al., 2006), so this chemokine might also play a role in monocyte transmigration of the CP.

The anatomical separation between the lesion site and the CP suggests this pathway as a potential general “route-phenotype orchestrating” mechanism for any CNS trauma and leukocyte type. In this regard, it is tempting to speculate that neutrophil activity may be similarly directed. These cells, recently acknowledged for their phenotypic diversity (termed N1–N2 in analogy to M1–M2), were reported as being either detrimental or beneficial to CNS recovery. In support, neutrophils are detected in the CSF and CP posttrauma (Szmydynger-Chodobska et al., 2009).

All together, our results suggest that the port of CNS entry determines the fate of the monocyte-macrophages maturing at the site of mechanical injury to the spinal cord. Entry through distinct gates of monocyte-macrophages that correspond to the known M1 and M2 waves at the lesion site might be a unique mechanism of CNS healing, and possibly of other immune-privileged sites, in which multiple entry routes exist. Such a discovery suggests the possibility of differential immune manipulation at the distinct ports as a therapeutic approach for acute and chronic CNS noninflammatory as well as inflammatory pathologies.

EXPERIMENTAL PROCEDURES

Animals

C57BL/6J, CD45.1, *Cx3cr1*$^{GFP/+}$ (Jung et al., 2000), and *Cd73*$^{-/-}$ (Fieschi and Sacchetti, 1967) mice were handled according to the regulations formulated by the Institutional Animal Care and Use Committee (IACUC).

Bone Marrow Radiation Chimeras

BM chimeras were prepared while shielding the head as detailed in Supplemental Experimental Procedures.

Spinal Cord Injury and Assessment of Functional Recovery

The SCs of deeply anesthetized mice were exposed by laminectomy at T12, and moderate contusive centralized injury (1.3 mm tip; 2 mm height; 2 mm/s) was inflicted (Infinite Horizon SC impactor; Precision Systems). Recovery was evaluated by hind-limb locomotor performance, according to the open-field BMS (Basso et al., 2006), as detailed in Supplemental Experimental Procedures.

Pharmacological Inhibition of CD73

Mice were injected both intraperitoneally (0.5 mg) and subcutaneously (0.5 mg) daily for a period of 7–14 days with α,β-methylene ADP (APCP; Sigma), a CD73 inhibitor (Synnestvedt et al., 2002).

Administration of Blocking Antibodies

Rat antibodies directed to VLA-4 (PS/2; 50 μg per mouse), VCAM-1 (M/K 2.7; 200 μg per mouse), or CD11b (M1/70; 100 μg per mouse) were intravenously injected, and Hamster

CCL2 antibody (2H5; 100 μg per mouse) was intraperitoneally injected, as detailed in Supplemental Experimental Procedures. Isotype-matched antibody served as a control, according to the manufacturer's recommendations (Bio Express).

CSF Collection

CSF was collected by the cisterna magna puncture technique, as detailed in Supplemental Experimental Procedures. Pooled samples (9–12 mice; 5 μl each) of equivalent volumes were analyzed, and results were normalized to 100 μl.

Intracerebroventricular Stereotactic Injections

Location of designated point: depth of 2.0 mm from brain surface, 0.4 mm posterior to the bregma, and 1.0 mm lateral to the midline. Monocytes (0.5×10^6 cells; isolated BM; >80% $Ly6c^{hi}$) were injected in PBS (3 μl; 1 μl per min). PBS served as a control.

CSF Flow Obstruction

Growth factor reduced Matrigel (BD Bioscience; 20 μl) was intracisternally injected. MRI check confirmed ventricle dilation. This procedure did not cause an inflammatory response at the needle puncture site, surrounding the ventricles, in the SC, or in the leptomeninges (Figure S4; Slobodian et al., 2007).

Adoptive Transfer of Monocytes

$CD115^+$ monocytes were isolated from BM, as detailed in Supplemental Experimental Procedures.

Statistical Analysis

Student's t test was used to compare two groups, and one-way ANOVA to compare several groups, followed by the Fisher LSD procedure (*p = 0.05). For multiple analyses of several groups, two-way ANOVA was done, followed by Bonferroni test. Repeated-measures ANOVA was used for BMS scoring, and follow-up by contrast t test (*p = 0.05). Results are presented as mean ± SEM; y axis error bars indicate SEM. Whenever pooled samples were used, the statistical analysis was based on the number of replicate pools without considering the animal number comprising the pools.

Supplementary Material

Refer to Web version on PubMed Central for supplementary material.

Acknowledgments

We thank L. Thompson for her generous gift of CD73 genetically ablated mice, S. Schwarzbaum for proofreading, and C. Raposo, G. Kunis, and M. Azulai for technical assistance. The work was supported in part by ISF-Legacy-Bio-Med program and the ERC Advanced grant. R.S., under the supervision of M.S., conceived the general ideas for this study and wrote the manuscript. R.S. in collaboration with O.M., G.Y., and N.R. or A.L. designed and performed experiments as well as conducted data analysis, with the assistance of J.R., E.K., V.K., and P.B. S.J. advised regarding monocytes.

References

Ajami B, Bennett JL, Krieger C, Tetzlaff W, Rossi FM. Local self-renewal can sustain CNS microglia maintenance and function throughout adult life. Nat Neurosci. 2007; 10:1538–1543. [PubMed: 18026097]

Anandasabapathy N, Victora GD, Meredith M, Feder R, Dong B, Kluger C, Yao K, Dustin ML, Nussenzweig MC, Steinman RM, Liu K. Flt3L controls the development of radiosensitive dendritic cells in the meninges and choroid plexus of the steady-state mouse brain. J Exp Med. 2011; 208:1695–1705. [PubMed: 21788405]

Arnold L, Henry A, Poron F, Baba-Amer Y, van Rooijen N, Plonquet A, Gherardi RK, Chazaud B. Inflammatory monocytes recruited after skeletal muscle injury switch into antiinflammatory macrophages to support myogenesis. J Exp Med. 2007; 204:1057–1069. [PubMed: 17485518]

Bartholomäus I, Kawakami N, Odoardi F, Schläger C, Miljkovic D, Ellwart JW, Klinkert WE, Flügel-Koch C, Issekutz TB, Wekerle H, Flügel A. Effector T cell interactions with meningeal vascular structures in nascent autoimmune CNS lesions. Nature. 2009; 462:94–98. [PubMed: 19829296]

Basso DM, Fisher LC, Anderson AJ, Jakeman LB, McTigue DM, Popovich PG. Basso Mouse Scale for locomotion detects differences in recovery after spinal cord injury in five common mouse strains. J Neurotrauma. 2006; 23:635–659. [PubMed: 16689667]

Bönner F, Borg N, Burghoff S, Schrader J. Resident cardiac immune cells and expression of the ectonucleotidase enzymes CD39 and CD73 after ischemic injury. PLoS ONE. 2012; 7:e34730. [PubMed: 22514659]

Boven LA, Van Meurs M, Van Zwam M, Wierenga-Wolf A, Hintzen RQ, Boot RG, Aerts JM, Amor S, Nieuwenhuis EE, Laman JD. Myelin-laden macrophages are anti-inflammatory, consistent with foam cells in multiple sclerosis. Brain. 2006; 129:517–526. [PubMed: 16364958]

Chinnery HR, Ruitenberg MJ, McMenamin PG. Novel characterization of monocyte-derived cell populations in the meninges and choroid plexus and their rates of replenishment in bone marrow chimeric mice. J Neuropathol Exp Neurol. 2010; 69:896–909. [PubMed: 20720507]

Fieschi A, Sacchetti C. Physiopathological and clinical aspects of hypersplenism Summary. Minerva Med. 1967; 58:4684–4688. [PubMed: 5583013]

Gordon S, Taylor PR. Monocyte and macrophage heterogeneity. Nat Rev Immunol. 2005; 5:953–964. [PubMed: 16322748]

Jung S, Aliberti J, Graemmel P, Sunshine MJ, Kreutzberg GW, Sher A, Littman DR. Analysis of fractalkine receptor CX(3)CR1 function by targeted deletion and green fluorescent protein reporter gene insertion. Mol Cell Biol. 2000; 20:4106–4114. [PubMed: 10805752]

Kalderon N. Cell elimination as a strategy for repair in acute spinal cord injury. Curr Pharm Des. 2005; 11:1237–1245. [PubMed: 15853680]

Kigerl KA, Gensel JC, Ankeny DP, Alexander JK, Donnelly DJ, Popovich PG. Identification of two distinct macrophage subsets with divergent effects causing either neurotoxicity or regeneration in the injured mouse spinal cord. J Neurosci. 2009; 29:13435–13444. [PubMed: 19864556]

Kleinewietfeld M, Puentes F, Borsellino G, Battistini L, Rötzschke O, Falk K. CCR6 expression defines regulatory effector/memory-like cells within the CD25(+)CD4+ T-cell subset. Blood. 2005; 105:2877–2886. [PubMed: 15613550]

Le Borgne M, Etchart N, Goubier A, Lira SA, Sirard JC, van Rooijen N, Caux C, Aït-Yahia S, Vicari A, Kaiserlian D, Dubois B. Dendritic cells rapidly recruited into epithelial tissues via CCR6/CCL20 are responsible for CD8+ T cell crosspriming in vivo. Immunity. 2006; 24:191–201. [PubMed: 16473831]

Mildner A, Schmidt H, Nitsche M, Merkler D, Hanisch UK, Mack M, Heikenwalder M, Brück W, Priller J, Prinz M. Microglia in the adult brain arise from Ly-6ChiCCR2+ monocytes only under defined host conditions. Nat Neurosci. 2007; 10:1544–1553. [PubMed: 18026096]

Mildner A, Mack M, Schmidt H, Brück W, Djukic M, Zabel MD, Hille A, Priller J, Prinz M. CCR2+Ly-6Chi monocytes are crucial for the effector phase of autoimmunity in the central nervous system. Brain. 2009; 132:2487–2500. [PubMed: 19531531]

Mills JH, Thompson LF, Mueller C, Waickman AT, Jalkanen S, Niemela J, Airas L, Bynoe MS. CD73 is required for efficient entry of lymphocytes into the central nervous system during experimental

autoimmune encephalomyelitis. Proc Natl Acad Sci USA. 2008; 105:9325–9330. [PubMed: 18591671]

Mills JH, Alabanza LM, Mahamed DA, Bynoe MS. Extracellular adenosine signaling induces CX3CL1 expression in the brain to promote experimental autoimmune encephalomyelitis. J Neuroinflammation. 2012; 9:193. [PubMed: 22883932]

Nahrendorf M, Swirski FK, Aikawa E, Stangenberg L, Wurdinger T, Figueiredo JL, Libby P, Weissleder R, Pittet MJ. The healing myocardium sequentially mobilizes two monocyte subsets with divergent and complementary functions. J Exp Med. 2007; 204:3037–3047. [PubMed: 18025128]

Noble LJ, Wrathall JR. Distribution and time course of protein extravasation in the rat spinal cord after contusive injury. Brain Res. 1989; 482:57–66. [PubMed: 2706482]

Radojicic M, Nistor G, Keirstead HS. Ascending central canal dilation and progressive ependymal disruption in a contusion model of rodent chronic spinal cord injury. BMC Neurol. 2007; 7:30. [PubMed: 17822568]

Ransohoff RM, Kivisäkk P, Kidd G. Three or more routes for leukocyte migration into the central nervous system. Nat Rev Immunol. 2003; 3:569–581. [PubMed: 12876559]

Rapalino O, Lazarov-Spiegler O, Agranov E, Velan GJ, Yoles E, Fraidakis M, Solomon A, Gepstein R, Katz A, Belkin M, et al. Implantation of stimulated homologous macrophages results in partial recovery of paraplegic rats. Nat Med. 1998; 4:814–821. [PubMed: 9662373]

Reboldi A, Coisne C, Baumjohann D, Benvenuto F, Bottinelli D, Lira S, Uccelli A, Lanzavecchia A, Engelhardt B, Sallusto F. C-C chemokine receptor 6-regulated entry of TH-17 cells into the CNS through the choroid plexus is required for the initiation of EAE. Nat Immunol. 2009; 10:514–523. [PubMed: 19305396]

Saederup N, Cardona AE, Croft K, Mizutani M, Cotleur AC, Tsou CL, Ransohoff RM, Charo IF. Selective chemokine receptor usage by central nervous system myeloid cells in CCR2-red fluorescent protein knock-in mice. PLoS ONE. 2010; 5:e13693. [PubMed: 21060874]

Schnell L, Fearn S, Klassen H, Schwab ME, Perry VH. Acute inflammatory responses to mechanical lesions in the CNS: differences between brain and spinal cord. Eur J Neurosci. 1999; 11:3648–3658. [PubMed: 10564372]

Sedgwick JD, Schwender S, Imrich H, Dörries R, Butcher GW, ter Meulen V. Isolation and direct characterization of resident microglial cells from the normal and inflamed central nervous system. Proc Natl Acad Sci USA. 1991; 88:7438–7442. [PubMed: 1651506]

Shechter R, London A, Varol C, Raposo C, Cusimano M, Yovel G, Rolls A, Mack M, Pluchino S, Martino G, et al. Infiltrating blood-derived macrophages are vital cells playing an anti-inflammatory role in recovery from spinal cord injury in mice. PLoS Med. 2009; 6:e1000113. [PubMed: 19636355]

Shechter R, Raposo C, London A, Sagi I, Schwartz M. The glial scar-monocyte interplay: a pivotal resolution phase in spinal cord repair. PLoS ONE. 2011; 6:e27969. [PubMed: 22205935]

Slobodian I, Krassioukov-Enns D, Del Bigio MR. Protein and synthetic polymer injection for induction of obstructive hydrocephalus in rats. Cerebrospinal Fluid Res. 2007; 4:9. [PubMed: 17894867]

Streilein JW. Ocular immune privilege: therapeutic opportunities from an experiment of nature. Nat Rev Immunol. 2003; 3:879–889. [PubMed: 14668804]

Sun X, Wang X, Chen T, Li T, Cao K, Lu A, Chen Y, Sun D, Luo J, Fan J, et al. Myelin activates FAK/Akt/NF-kappaB pathways and provokes CR3-dependent inflammatory response in murine system. PLoS ONE. 2010; 5:e9380. [PubMed: 20186338]

Synnestvedt K, Furuta GT, Comerford KM, Louis N, Karhausen J, Eltzschig HK, Hansen KR, Thompson LF, Colgan SP. Ecto-5′-nucleotidase (CD73) regulation by hypoxia-inducible factor-1 mediates permeability changes in intestinal epithelia. J Clin Invest. 2002; 110:993–1002. [PubMed: 12370277]

Szmydynger-Chodobska J, Strazielle N, Zink BJ, Ghersi-Egea JF, Chodobski A. The role of the choroid plexus in neutrophil invasion after traumatic brain injury. J Cereb Blood Flow Metab. 2009; 29:1503–1516. [PubMed: 19471279]

Szmydynger-Chodobska J, Strazielle N, Gandy JR, Keefe TH, Zink BJ, Ghersi-Egea JF, Chodobski A. Posttraumatic invasion of monocytes across the blood-cerebrospinal fluid barrier. J Cereb Blood Flow Metab. 2012; 32:93–104. [PubMed: 21829211]

Takigawa T, Yonezawa T, Yoshitaka T, Minaguchi J, Kurosaki M, Tanaka M, Sado Y, Ohtsuka A, Ozaki T, Ninomiya Y. Separation of the perivascular basement membrane provides a conduit for inflammatory cells in a mouse spinal cord injury model. J Neurotrauma. 2010; 27:739–751. [PubMed: 20038195]

Thomson LF, Ruedi JM, Glass A, Moldenhauer G, Moller P, Low MG, Klemens MR, Massaia M, Lucas AH. Production and characterization of monoclonal antibodies to the glycosyl phosphatidylinositol-anchored lymphocyte differentiation antigen ecto-5′-nucleotidase (CD73). Tissue Antigens. 1990; 35:9–19. [PubMed: 2137649]

Wilbanks GA, Streilein JW. Fluids from immune privileged sites endow macrophages with the capacity to induce antigen-specific immune deviation via a mechanism involving transforming growth factor-beta. Eur J Immunol. 1992; 22:1031–1036. [PubMed: 1551403]

Yin Y, Henzl MT, Lorber B, Nakazawa T, Thomas TT, Jiang F, Langer R, Benowitz LI. Oncomodulin is a macrophage-derived signal for axon regeneration in retinal ganglion cells. Nat Neurosci. 2006; 9:843–852. [PubMed: 16699509]

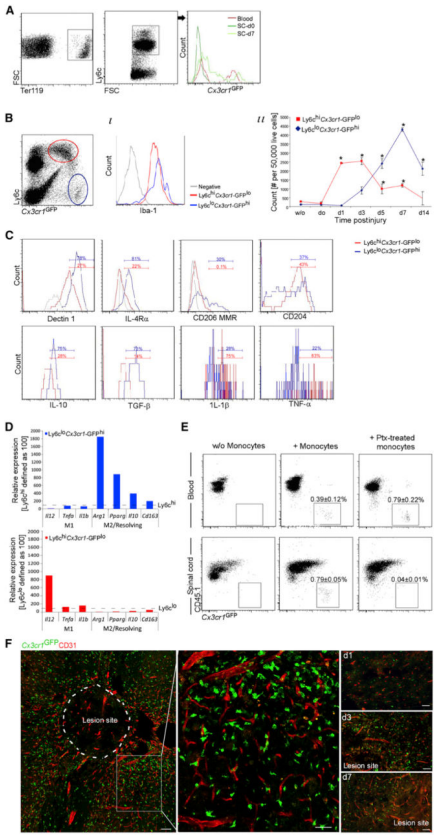

Figure 1. M1 and M2 Monocyte-Macrophages Are Actively Recruited to Injured SC Parenchyma

(A–C) Flow cytometry analysis of lesion sites of injured *Cx3cr1*$^{GFP/+}$ chimeras.

(A) Erythrocytes and GFP^{+} monocyte-macrophages (n = 3–5 mice).

(B) M1 and M2 monocyte-macrophage populations (based on GFP and Ly6c). (i) Histogram for Iba-1. (ii) Quantitative kinetic analysis. ANOVA: $F_{13,27} = 19.5$, *p = 0.0001 relative to uninjured.

(C) Pooled (n = 10–20) lesion sites (d7) analyzed for M1 and M2 markers and intracellular cytokines.

(D) Monocyte-macrophage populations were separately sorted by flow cytometry from the lesion parenchyma (d5; n = 20 chimeras) and analyzed by qRT-PCR. The same experimental results were used, but each graph is presented relative to the expression of the reciprocal subset, defined as 100.

(E) Analysis of CD45.1 injured mice, 3 days after SCI and 2 days after i.v. injection of monocytes (i.v. at d1; *Cx3cr1*$^{GFP/+}$; with or without pertussis toxin [ptx] pretreatment). Student's t test, n = 3 pools (of 2 mice) in each group: blood p = 0.197, SC p = 0.0001. Cells were Ly6c pregated.

(F) *Cx3cr1*$^{GFP/+}$ chimeras SC stained for GFP and CD31. n = 4 mice per time point, three depths. Data are represented as mean ± SEM. Scale bars represent 50 μm.

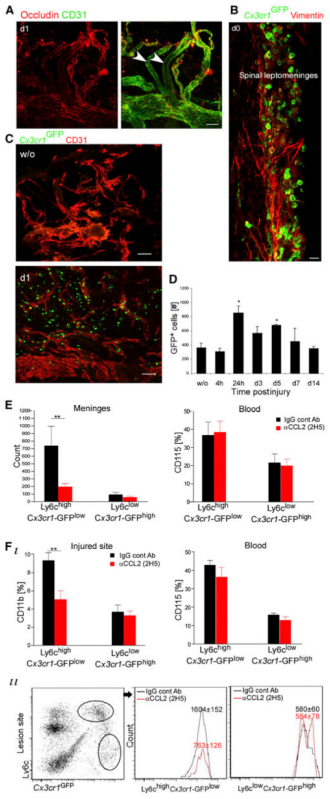

Figure 2. CCL2-Dependent Homing of M1 Monocyte-Macrophages to the Injured SC via the Leptomeninges

(A) SC leptomeninges stained for occludin and CD31. Arrowheads indicate vessels lacking tight junctions. n = 4 mice.

(B) GFP^+ cells in the leptomeninges of SC sections of injured *Cx3cr1*$^{GFP/+}$ chimeras. n = 4 mice.

(C) Whole-mount staining of SC leptomeninges dissected out from *Cx3cr1*$^{GFP/+}$ chimeras. n = 4 mice per time point.

(D) Quantification by flow-cytometric analysis of GFP^+ cells in dissected SC leptomeninges lining the injured site. Values are absolute cell numbers per 10,000 live cells. ANOVA: $F_{6,14} = 4.26$, *p = 0.011 relative to uninjured.

(E and F) Spinally injured *Cx3cr1*$^{GFP/+}$ chimeras, intraperitoneally injected with CCL2 (or isotype-matched IgG) antibodies, analyzed on d1 for SC leptomeninges (E) or at d5 for lesion sites (F). CCL2 inhibition reduced Ly6c^{hi}*Cx3cr1*-GFP^{lo} trafficking. Two-way ANOVA: (E) n = 5–6 mice; $F_{1,17} = 8.2$, p = 0.01; (F) n = 4–7 mice; $F_{1,17} = 8.8$, p = 0.008. Values are absolute cell numbers in 0.5 cm SC tissue. As a control, blood was analyzed by two-way ANOVA: (E) $F_{1,16} = 0$, p = 0.96; (F) $F_{1,20} = 1.8$, p = 0.2.

Data are represented as mean ± SEM. Scale bars represent 100 μm in (A) and (C) and 10 μm in (B). See also Figure S1.

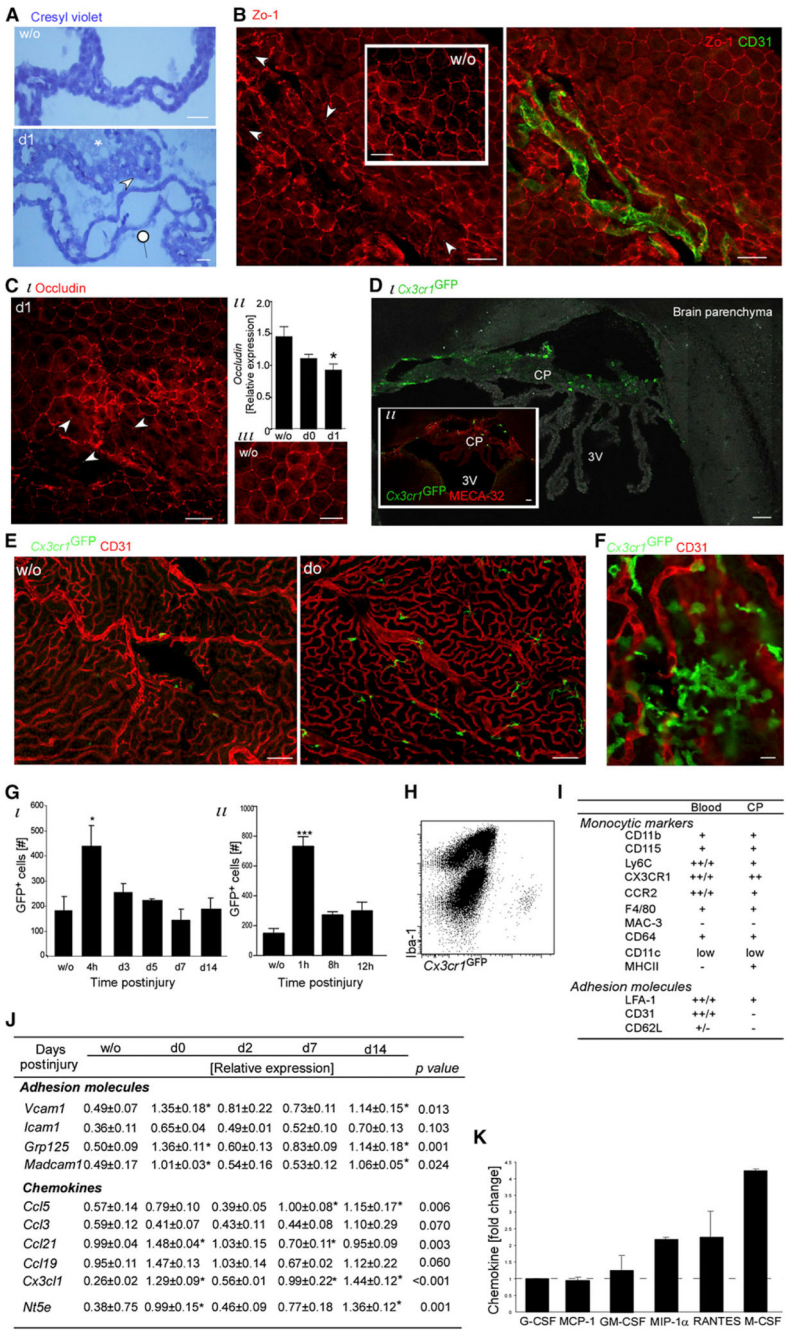

Figure 3. SCI Leads to Brain Choroid Plexus Activation and Monocyte Recruitment

(A–C) Morphological changes at the CP after SCI.

(A) Cresyl violet staining; arrowheads indicate epithelial swelling, pointer indicates epithelial flattening or attenuation, and asterisk indicates ventricular flocculent material. n = 3–4 animals.

(B and C) Staining of CP for tight junctions (Zo-1 in B and occludin in C) and CD31. Arrowheads mark areas with disorganized epithelial tight junctions. n = 3 animals per time point; qualitatively similar. (Cii) qRT-PCR analysis of isolated CP for *Ocln*, encoding

occludin. n = 3–4 per time point. ANOVA: F = 6, p = 0.03. (D–I) GFP^+ cells in the CP of SC-injured *Cx3cr1*$^{GFP/+}$ chimeras.

(D–F) GFP^+ cells in CP sections (D) or whole mounts (E and higher magnification in F). n = 3–4 mice.

(G–I) Flow cytometry analysis.

(G) Quantitative kinetics. Values are absolute cell numbers per 10,000 live cells. ANOVA: (i) $F_{5,12} = 3.12$, p = 0.04; (ii) $F_{3,15} = 27.05$, *p < 0.0001 relative to uninjured.

(H) Dot plot of CP (d0; chimera) for Iba-1 and GFP.

(I) Marker expression; slash indicates heterogeneity; isotype controls served as negative controls; pools of ten mice.

(J and K) CPs analyzed by (J) qRT-PCR (n = 3–4 per time point; ANOVA; *relative to uninjured) and (K) Luminex (pools of six mice; results of day 0 are presented as fold of change relative to noninjured; ANOVA; $F_{6,9} = 4.96$, p = 0.018).

Data are represented as mean ± SEM. Scale bars represent 100 μm in (D) and (E), 50 μm in (A)–(C), and 10 μm in (F). See also Figure S2.

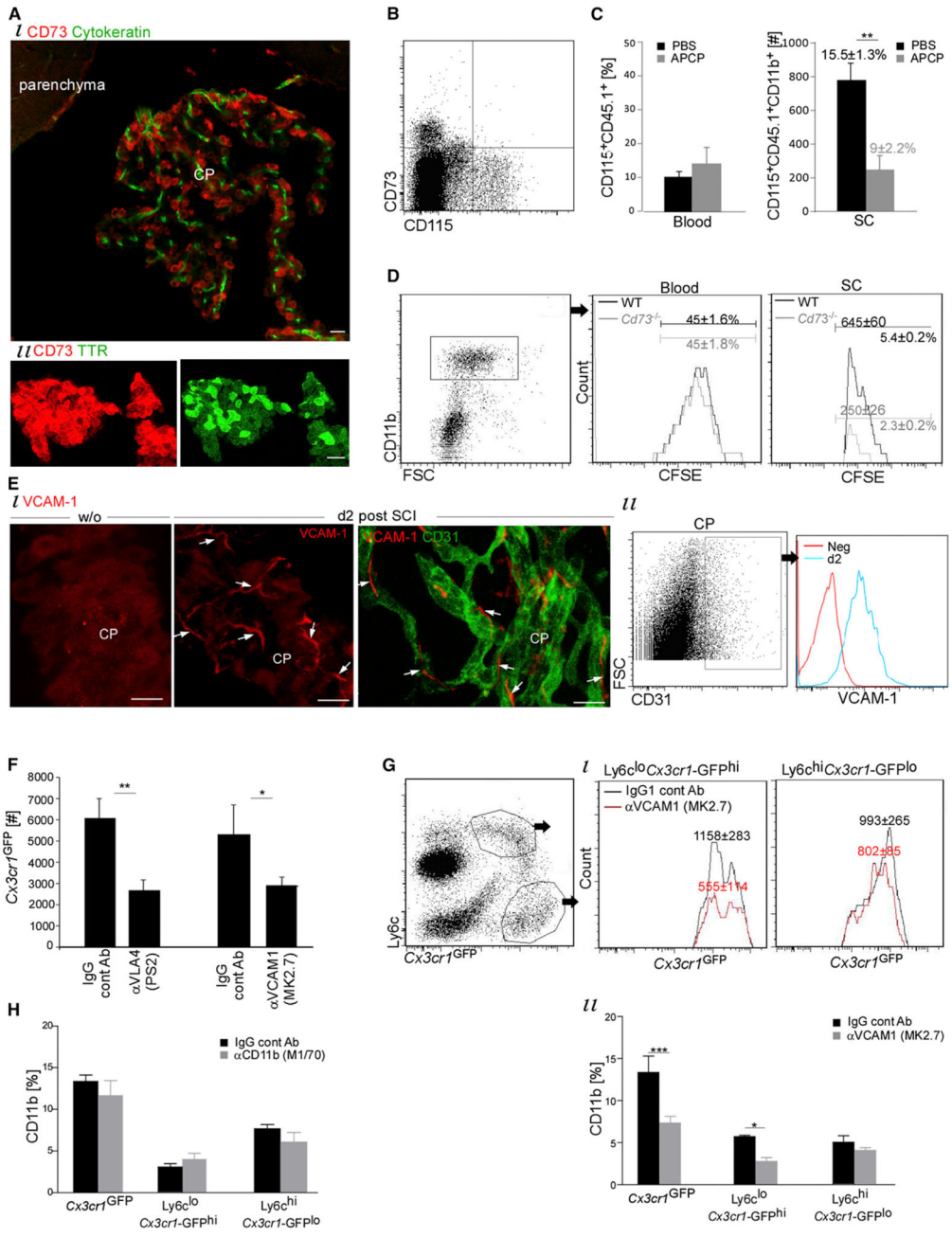

Figure 4. CP CD73 and VCAM-1 Orchestrate the Trafficking of Monocytes Maturing into M2 at the Injured SC Site

(A and B) CD73 expression by CP epithelium (A) and not by blood CD115^{+} monocytes (B) of spinally injured mice.

(C) CD11b^{+}CD115^{+}CD45.1^{+} monocyte-macrophages in injured (d14) CD45.1→WT (CD45.2) chimeras, after treatment with APCP, a CD73 inhibitor. Student's t test: n = 5–7 mice; SC, p = 0.007; blood, p = 0.31; percentages are of CD11b.

(D) Monocyte-macrophages ($CD11b^+CFSE^+$) at the lesion site (d7) of *Cd73*$^{-/-}$ mice and their controls. Student's t test: n = 4–5 mice, p = 0.01. CFSE was i.v. injected 24 hr before injury. Values are absolute cell numbers in 0.5 cm SC tissue.

(E) VCAM-1 expression by CP endothelium after SCI (n = 3–4 mice).

(F and G) Monocyte-macrophages ($GFP^+Ly6c^+CD11b^+$) in injured *Cx3cr1*$^{GFP/+}$ chimeras (d5), i.v. injected with VLA-4 (PS2) or VCAM-1(MK2.7) or isotype-matched antibodies, as controls. n = 5 mice per group. Student's t test: (F) VLA-4 antibodies: p = 0.01; VCAM-1 antibodies: p = 0.03. (Gi) $Ly6c^{lo}$*Cx3cr1*-GFP^{hi} p = 0.01; $Ly6c^{hi}$*Cx3cr1*-GFP^{lo} p = 0.35. (Gii) Two-way ANOVA: $F_{1,23} = 17.24$, p = 0.0004. Values are absolute cell numbers in 0.5 cm SC tissue, per 20,000 $CD11b^+$ cells.

(H) Monocyte-macrophages ($GFP^+Ly6c^+CD11b^+$) in injured (d5) *Cx3cr1*$^{GFP/+}$ chimera SC, i.v. injected with CD11b (or isotype matched) antibodies. n = 6 per group. Two-way ANOVA: $F_{1,30} = 1.23$, p = 0.28.

Data are represented as mean ± SEM. Scale bars represent 50 μm in (Ai) and (E) and 20 μm in (Aii). See also Figure S3.

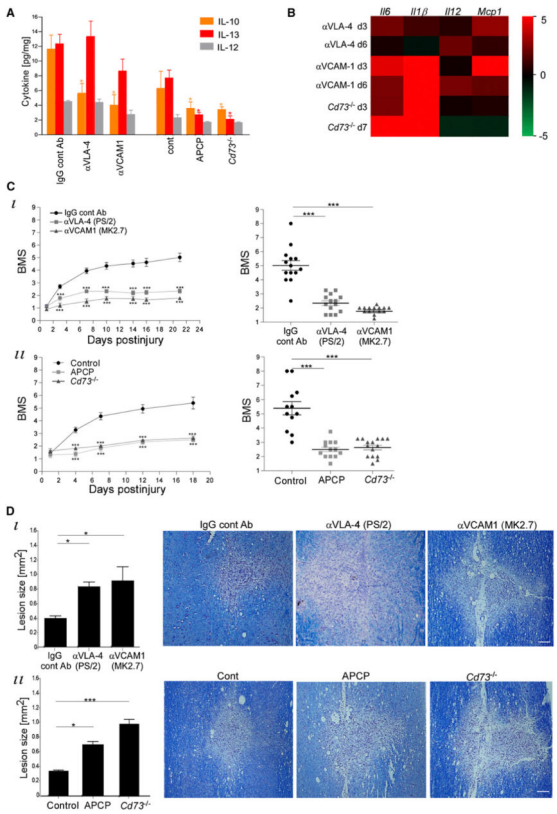

Figure 5. The CP-Dependent Recruited Cells Resolve Inflammation and Improve Recovery

VLA-4-VCAM-1 interaction (by VLA-4 or VCAM-1 antibodies) or CD73 activity (using APCP, or *Cd73*$^{-/-}$) was inhibited in SC-injured mice; appropriate controls were included.

(A) Cytokine Multiplex analysis of lesion site (d7). n = 4–8 pools of 3 mice. Two-way ANOVA: $F_{5,74} = 11.1$, $p < 0.0001$.

(B) qRT-PCR analysis of lesion sites for genes encoding proinflammatory cytokines, presented as a heat map relative to the relevant control.

(C) Hind limb motor function, assessed according to the BMS. Left: Motor score as a function of time. Right: Scores (d21) of individual mice. (i) n = 14–15 mice per group. Left: repeated ANOVA: $F_{\text{between groups}}(2,40) = 60.8$, $p < 0.0001$; right: ANOVA, $F = 59$, $p < 0.0001$. (ii) n = 12–15 mice per group. Left: repeated ANOVA: $F_{\text{between groups}}(2,37) = 36.7$, $p < 0.0001$; right: ANOVA: $F = 32$, $p < 0.0001$.

(D) Quantification of lesion size (d21; an average of 3 depths) and representative pictures, as demarcated by Luxol and Nissl reactivity in longitudinal coronal sections. n = 8–10 mice per group. ANOVA: (i) $F = 35$, $p = 0.02$; (ii) $F = 10.2$, $p = 0.0007$.

Data are represented as mean ± SEM. Scale bars represent 100 μm (D).

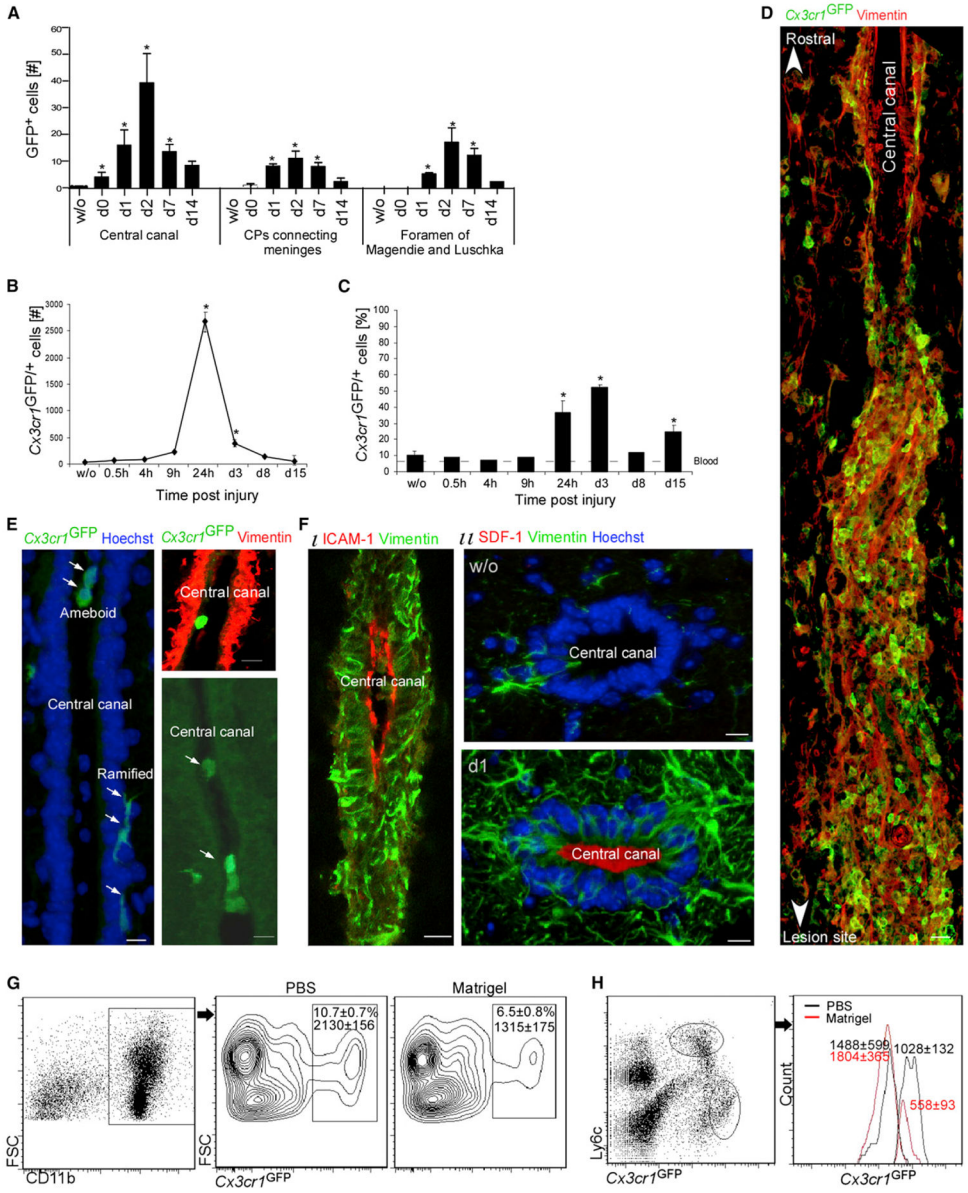

Figure 6. Homing of M2 Monocyte-Macrophages to the Injured Parenchyma through the Cerebrospinal Fluid

(A–C) Quantification of GFP$^+$ cells in *Cx3cr1*$^{GFP/+}$ chimeras after SCI (A) in sections (30 μm) of brains and SC. # in segments of 0.5 cm; n = 4–8 mice per time point. ANOVA: F = 4.7, *p < 0.0001 relative to uninjured.

(B) GFP$^+$ cell count in the CSF assessed by flow cytometry (results are presented as cell count per 100 μl CSF). n = 4–6 pools (of 8–12 mice); Student's t test; * relative to uninjured.

(C) GFP$^+$ cell count in the CSF presented as percentages of live cells, as determined by flow cytometry. Dashed line represents blood monocyte percentages. n = 4–6 pools (of 8–12 mice); Student's t test; * relative to uninjured.

(D) GFP$^+$ cells in association with vimentin-immunoreactive fiber structure at the edge of the central canal (delineated by Vimentin) of injured *Cx3cr1*$^{GFP/+}$ chimeras. n = 3 mice.

(E) SC sections immunostained for visualization of GFP^+ cells in the central canal (delineated by Vimentin or Hoechst) of injured *Cx3cr1*$^{GFP/+}$ chimeras. n = 3 mice each.
(F) Central canal stained for vimentin together with ICAM-1 (i) or SDF-1(ii).
(G and H) *Cx3cr1*$^{GFP/+}$ chimeras were subjected to SCI concurrently with intracisternal Matrigel injection, and at d7, their SC were analyzed for monocyte-macrophages. Student's t test: (G) n = 5–7 mice, p = 0.02; (H) n = 6–8 mice; Ly6c^{lo}*Cx3cr1*-GFP^{hi} p = 0.02; Ly6c^{hi}*Cx3cr1*-GFP^{lo} p = 0.66; one experiment representative of three. In (H), cells from both gates were plotted on the same histogram. Absolute numbers of cells in 0.5 cm SC tissue, per 20,000 $CD11b^+$ cells, are indicated.
Data are represented as mean ± SEM. Scale bars represent 20 μm in (D) and 10 μm in (E) and (F). See also Figure S4.

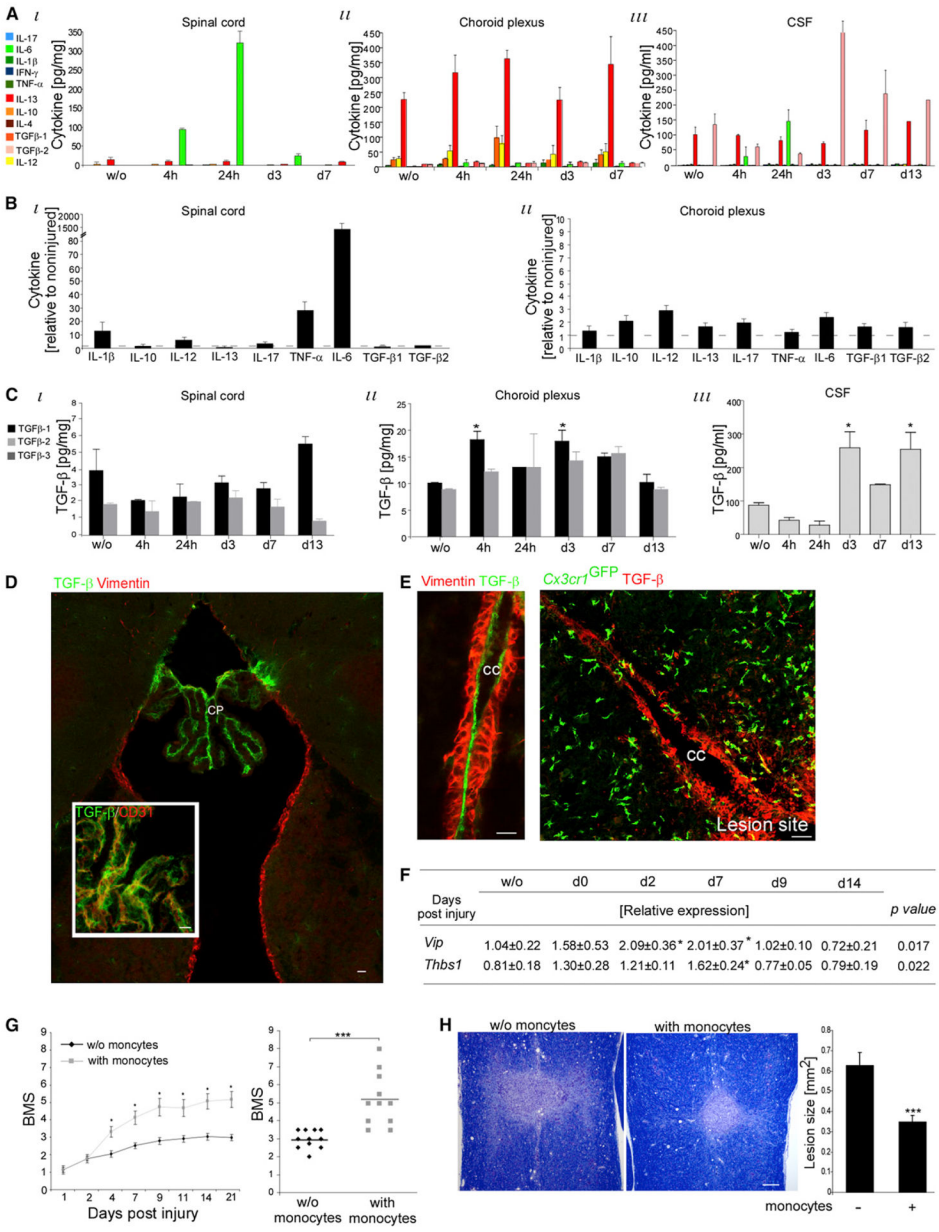

Figure 7. The CP-CSF Pathway Exhibits an M2-Supportive Milieu

(A–C) Luminex analysis of pooled (6–12 mice) samples of SC, CP, and CSF.

(A) Samples analyzed for pro- (green) and anti- (red) inflammatory cytokines. Two-way ANOVA: (i) $F = 32.1$, $p < 0.0001$; $F_{day} = 32.6$, $p < 0.0001$; $F_{cyto} = 65$, $p < 0.0001$; (ii) $F = 0.817$, $p = 0.73$; $F_{day} = 1.84$, $p = 0.13$; $F_{cyto} = 67.7$, $p < 0.0001$; (iii) $F = 1.82$, $p = 0.023$; $F_{day} = 0.78$, $p = 0.56$; $F_{cyto} = 13.9$, $p < 0.0001$.

(B) Fold increase at 24 hr postinjury relative to uninjured amount. ANOVA: (i) $F = 38$, $p < 0.0001$; (ii) $F = 3.05$, $p = 0.014$.

(C) TGF-β isoforms. Two-way ANOVA: (i) $F = 4.35$, $p = 0.017$; $F_{day} = 1.86$, $p = 0.17$; $F_{cyto} = 26$, $p = 0.0002$; (ii) $F = 0.67$, $p = 0.05$; $F_{day} = 3.9$, $p = 0.02$; $F_{cyto} = 2.5$, $p = 0.13$. ANOVA: (iii) $F = 12.14$, $p = 0.004$.

(D and E) TGF-β staining in (D) brain (n = 3 mice each; 3 depths, analyzed at d1, d3, and d7) or (E) central canal (CC; Vimentin^{+}) of injured mice; right: in *Cx3cr1*$^{GFP/+}$ chimeras (n = 3 mice).

(F) qRT-PCR expression of isolated CP. ANOVA: n = 3–4 mice per time group; *relative to uninjured.

(G and H) Injured C57BL/6 mice were ICV injected (d3) with CD115^{+} monocytes (isolated from BM; predominantly [>80%] Ly6c^{hi}).

(G) Hind limb motor function assessment according to BMS. Left: Kinetic follow up. Right: Motor scores (d21) of individuals. Left: Repeated ANOVA: $F_{\text{between groups}}(1,26) = 13$, $p = 0.001$. Right: Student's t test: n = 11 mice per group, $p = 0.0001$; repeated in three experiments.

(H) Lesion size evaluation (d28) as demarcated by Luxol and Nissl reactivity in longitudinal coronal sections. Student's t test: n = 9 mice per group, $p = 0.001$.

Data are represented as mean ± SEM. Scale bars represent 50 μm in (D), 20 μm in (E), and 100 μm in (H).